23rd Australasian Fluid Mechanics Conference - 23AFMC
Sydney, Australia
4 – 8 December 2022

Paper No: AFMC2022-129

# The effect of nuclei and gap height on cavitation in tip leakage flow.

**Patrick Russell[1*], Luka Barbaca[1], James Venning[1], Bryce Pearce[1] and Paul Brandner[1]**

[1] Australian Maritime College, The University of Tasmania, Launceston, TAS 7250, Australia
*mailto: patrick.russell@utas.edu.au

## Abstract

Cavitation in tip leakage flow is investigated experimentally in a variable pressure water tunnel using a single stationary hydrofoil analogy to that of rotating blading. The clearance between the hydrofoil tip and ceiling of the test section is varied for a gap height to maximum thickness ratio of between $\tau = h/t_{max} = 0.1$–$2$ for two polydisperse freestream nuclei populations at a chord-based Reynolds number of $Re = 3 \times 10^6$. The two populations are representative of the limits of nuclei populations experienced in practical flows. The first population is comprised of strong nuclei with large negative critical pressures that occur in low concentrations within the flow. For the second nuclei population the flow is abundantly seeded with microbubbles of low tensile strength. The hydrofoil model is similar to a NACA66 thickness form with a NACA $a = 0.8$ series camber curve and maintains a flat pressure distribution along most of the chord. The hydrofoil is tested for cavitation numbers from $\sigma = 1$–$6$, where $\sigma = (p - p_v)/0.5\rho U^2$ with $p$ is the static pressure at the tunnel ceiling, and $p_v$ is the water vapour pressure. Tests are repeated in one degree increments for $\alpha = 0$–$10°$. Data recorded are of simultaneous high-speed photography and hydrophone measurements, and are used to relate the cavitation topology to acoustic data. Variation in the leakage vortex trajectory with gap height and incidence are discussed, as visualised by bubble accumulation in the leakage vortex for the heavily nucleated flow. Developed cavitation dynamics are shown to vary greatly with the nuclei availability as well as tip clearance, with inception events becoming particularly violent for intermediate tip clearances.

## 1 Introduction

Flow between the tip of a rotating blade and a static casing, referred to as 'tip-leakage flow', is a feature observed in many fluid mechanics applications. It originates due to the pressure difference between the blade's pressure and suction sides. Due to the adverse effects that tip-leakage flow has on the performance of turbomachinery, namely; efficiency losses, rotating instabilities, cavitation and earlier onset of stall, the topic has been the focus of considerable research efforts for over a half-century (Chesnakas and Jessup, 2003; Dreyer *et al.*, 2014; Laborde *et al.*, 1997; Oweis and Ceccio, 2005; Oweis *et al.*, 2006a; Rains, 1954).

Despite this attention it remains a challenging problem in engineering design, particularly with regard to cavitation inception in pumps and ducted propulsors. The leakage flow rolls up to form a tip-leakage vortex (TLV), similar to the vortex classically observed at the tip of a finite span foil (Green, 1995). The core of the tip-leakage vortex is usually the region with the lowest mean pressure in the flow-field, and thus it has been generally considered as the likely site for the cavitation inception (Oweis *et al.*, 2006b). However, as shown by Oweis and Ceccio (2005) and Wu *et al.* (2011) using Particle Image Velocimetry (PIV), the tip-leakage flow is characterized by a complex unsteady flow-field. Recently, the interaction between secondary vorticity formed near the blade tip and the primary tip-leakage vortex has received particular attention due to unsteady stretching of the smaller vortical filaments. It has been shown that during interaction with the primary TLV this stretching can lead to a brief but intense drop in pressure at the core of the vortex filament, with an instantaneous pressures much lower than the TLV (Chang *et al.*, 2012; Oweis and Ceccio, 2005). Consequently, cavitation inception may occur at higher free-stream pressures than might otherwise be expected.

In practical flows inception of cavitation requires the presence of a site of weakness, i.e. a cavitation nuclei. In the absence of nuclei water can be in tension and sustain large negative pressures (Temperley and Ll, 1946). A substantial body of literature exists reporting on the effects of tip gap clearance, Reynolds number, and the thickness of the in-flowing boundary layer. However interactions between these features on inception the effect of freestream nuclei content has not received significant attention. The current understanding of this aspect has largely been inferred from other contexts (Chang *et al.*, 2012) or solely from simulation (Hsiao and Chahine, 2008). To assess the influence of nuclei inception and developed cavitation in tip leakage flows, an analogy to a rotating tip leakage using a stationary hydrofoil has been studied in the variable pressure water tunnel at the Australian Maritime College – Cavitation Research Laboratory (CRL). Tip gap flow is developed between the ceiling of the test section and the tip of a hydrofoil mounted rigidly to the floor. The nuclei content in the water is carefully controlled using the tunnel architecture and ancillary systems (Khoo *et al.*, 2020). Prior studies performed in this facility using a NACA 0012 hydrofoil model equipped with interchangeable square-edge tips, revealed issues with premature cavitation in the gap, local sources of nucleation at the discontinuity between the tip and the hydrofoil main body and sheet cavitation at the base due to the use of a thicker NACA 0040 foil section to prevent model vibration (Russell *et al.*, 2020a,c). In order to mitigate these issues, a new hydrofoil model with a custom-designed cambered section and a complex tip rounding, has been designed for the present work. In addition, a new experimental apparatus has been developed enabling continuous adjustment of the hydrofoil incidence and the tip clearance. Cavitation inception for the optimised hydrofoil was explored for two nuclei populations: The natural (or background) nuclei population, ever present in the tunnel (Khoo *et al.*, 2020), and an abundant polydisperse population of comparatively large nuclei from which the flow has been artificially seeded (Russell *et al.*, 2020b). These populations represent the two extremes in which turbomachinery and ducted propulsors may operate.

This work isolates and characterises the visual and acoustic differences from cavitation inception with different freestream nuclei populations as they change with gap height in tip-leakage flow. The variation of the tip gap in these experiments alters the path of the leakage vortex due to the presence of the wall and its boundary layer. Results also capture the trajectory of the vortex with gap height and incidence.

## 2 Experiment Setup

Experiments were performed in the Australian Maritime College variable pressure water tunnel at a chord-based Reynolds number of $Re = Uc/\nu = 3 \times 10^6$, where $U$ is the mean flow velocity and $\nu$ is the water kinematic viscosity. During testing the cavitation number was varied from $\sigma$ = 1–6, where we define $\sigma = (p - p_v)/0.5\rho U^2$, with $p$ is the static pressure at the tunnel ceiling, $p_v$ is the water vapour pressure and $\rho$ is the water density. The hydrofoil clearance was non-dimensionalised by the maximum thickness of the hydrofoil tip section, $\tau = h/t$, such that measurements were taken at $\tau = \{0.1, 0.2, 0.4, 0.6, 0.8, 1.0, 1.4, 1.8\}$, and were repeated in one degree increments for $\alpha$ = 0–10°.

A schematic of the arrangement developed to study cavitation in the gap flow between a stationary hydrofoil and the ceiling of the tunnel test-section is represented in figure 1. The tunnel test-section is $0.6 \times 0.6$ m square at the entrance, by 2.6 m long. The test-section ceiling is horizontal with the floor sloping 20 mm over the length to maintain nominally constant speed and a zero-stream-wise pressure gradient. The operating velocity and pressure are controlled independently, with ranges from 2 to 13 m/s and 4 to 400 kPa absolute, respectively. The tunnel volume is 365 m$^3$ and is filled with demineralised water. Optical access is provided through acrylic windows on each side of the test-section. Details on the facility in general can be found in Brandner *et al.* (2006, 2007).

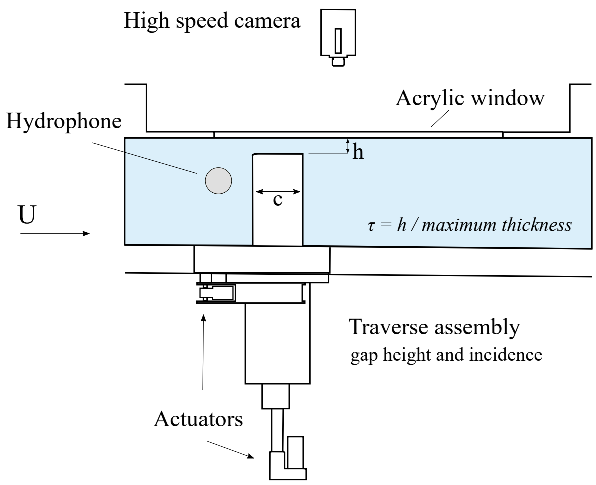


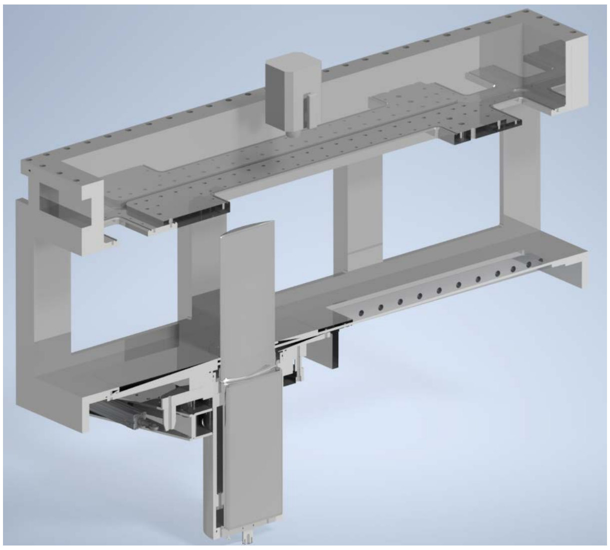

**Figure 1.** a) Schematic of the model within test section of the cavitation tunnel. b) 3D model render of the hydrofoil model and actuator assembly.

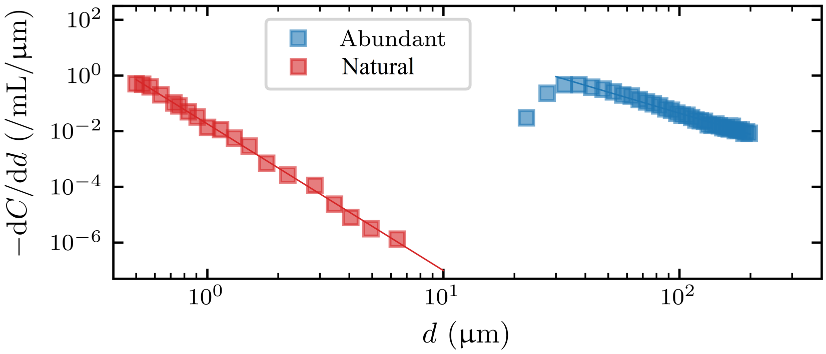


**Figure 2.** Cumulative size distribution of the natural and abundant poly-disperse populations used for characterization of the effect of nuclei on the TLF.

The experiments were performed for a natural nuclei population and for an abundant polydisperse population generated via artificial seeding of the tunnel water with microbubbles. The tunnel natural nuclei population was characterized by Khoo *et al.* (2020) using measurements acquired via mechanical activation in a Cavitation Susceptibility Meter (CSM). They demonstrated that this population is practically invariant to tunnel operating conditions for dissolved oxygen levels below 4 ppm. Current experiments were performed with a dissolved $O_2$ content between 2.75 and 3.5 ppm.

Microbubbles for artificial nuclei seeding are generated via rapid depressurization of supersaturated water through an orifice, with a device referred to as 'mini-tube' (Barbaca *et al.*, 2020). An array of 10 mini-tube devices was utilized to generate a nuclei plume seeding the top third of the test section and 50 mm each side of the tunnel centre line. Each device produces microbubbles at a rate of $\approx 10^6$ Hz. The resulting nuclei population in the test-section was characterized by Russell *et al.* (2020b) using Mie-Scattering Imaging (MSI). Cumulative size distributions for the both, natural and abundant, nuclei populations are given in figure 2.

The hydrofoil and mounting block are made out of a single forged stainless steel billet. The hydrofoil has a chord of $c = 280$ mm, and the span can be varied between $s = 540$ mm and 610 mm. The use of a NACA 66-012 mod section analogy at the tip, results with a tip thickness, $t = 33.6$ mm. See (Russell *et al.*, 2022) for a description of the development of the hydrofoil geometry. The hydrofoil tapers towards the root, with the maximum root thickness of 67.2 mm. A 90 mm long parallel section is added between the hydrofoil root and the mounting block to ensure a streamlined flow along the foil/wall junction as the hydrofoil is traversed in the vertical direction. The traversing assembly allows for a continuous adjustment of the tip gap ($h$) and the incidence ($\alpha$) of the hydrofoil. For the present work the gap could be adjusted in the range $1 \leq h \leq 70$ mm and the incidence in the range $-10^{\circ} \leq \alpha \leq 10^{\circ}$. The gap and the incidence adjustments were controlled using Tolomatic 32RSA-HT1 stepper motor electric linear actuators, driven by a Tolomatic ACS stepper driver motor controller, with a maximum thrust of 18.5 kN. The actuators have an accuracy of 0.01 mm across a 300 mm travel. The hydrofoil leading edge is located $\approx 900$ mm downstream of the test-section entrance with the unperturbed incoming wall boundary layer thickness of $\delta_{99} = 19$ mm (the thickness where the local velocity reaches 99% of the freestream). In these experiments $\alpha$ was varied from $0^{\circ}$ to $10^{\circ}$ to cover a range from lightly loaded conditions all the way to near stall of the tip section profile in 2D flow.

High-speed imaging of the cavitation topology in the gap was acquired using a Phantom v2640 camera with a maximum resolution of 2048 $\times$ 1952 pixels, mounted above the tunnel test section. The camera was equipped with a Nikon AF Nikkor 24 mm f/2.8 D lens with the images acquired at a cropped resolution of 2048 $\times$ 640 pixels at a sampling rate of 10000 frames per second. Continuous illumination was provided from two Effilux EFFI-BL-LITE-1M12P 650 $\times$ 650 mm LED panels mounted to the side of the test section and three Veritas Constellation 120 LED lamps mounted above and to the side of the test section. The image acquisition was controlled via Phantom PCC 3.4.4 software. Optical access to the gap was provided through a 1150 mm long $\times$ 215 mm wide acrylic window in the test section ceiling.

Acoustic measurements were obtained using a Brüel & Kjær Type 8103 hydrophone (voltage sensitivity 25.1 $\mu$V/Pa) mounted in a flooded cavity (kept at the same pressure as the tunnel test section) beneath a 10 mm polyurethane diaphragm, with a 149 mm sensing diameter (Doolan *et al.*, 2013). The hydrophone was mounted in the side wall, 150 mm below the ceiling and approximately a chord length upstream of the hydrofoil leading edge. The signal was conditioned using a Brüel & Kjær Nexus conditioner and amplifier, which was also used to apply a 0.1 Hz - 100 kHz bandpass filter. The filtered signal was acquired using a National Instruments PXIe-4497 card at a sampling rate of 204.8 kS/s. Each acoustic measurement was performed for a period of 60 s.

The high-speed imaging and the acoustic measurements were triggered independently, however, the data was synchronized by recording the camera trigger signal along with the acoustics and using it to align the two data sets. The camera was operated with a post trigger, so that once an incipient event was manually observed or heard, the camera trigger could be activated.

### 2.1 Results

A comparison of the cavitation topology and acoustic signature of the tip-leakage flow at $\alpha = 6^{\circ}$ and $\tau = 0.8$ for both the natural nuclei and seeded flow is presented in figure 4. In the top left quadrant of the figure, sample image pairs are presented for both nuclei concentrations at three cavitation numbers, $\sigma = \{2,\ 4,\ 6\}$. A small segment of the hydrophone measurements that accompany these images are plotted below (bottom left quadrant). These have been band-pass filtered with cutoff frequencies of 1–5 kHz. Together they show that for flow with a sparse population of nuclei — as in the natural (background) nuclei population — cavitation occurs as discrete events. For the majority of conditions tested it was observed that the leading edge of an isolated cavity is advected downstream rather slowly. As the cavity in the leakage vortex attempts to expand upstream along the vortex core it's progress is in competition with the global downstream movement of the flow. Just below incipient values such events disappear completely before a new event occurs. When pressures in the flow are well below inception, the leading edge of the cavity will often persist within the vicinity of the hydrofoil trailing edge over a protracted period of time. This can enable a second event to occur upstream in the tip leakage vortex while a prior cavity is still present (see the top image in figure 4). The trailing edge of a growing cavity does not need to contend with the oncoming flow and rapidly

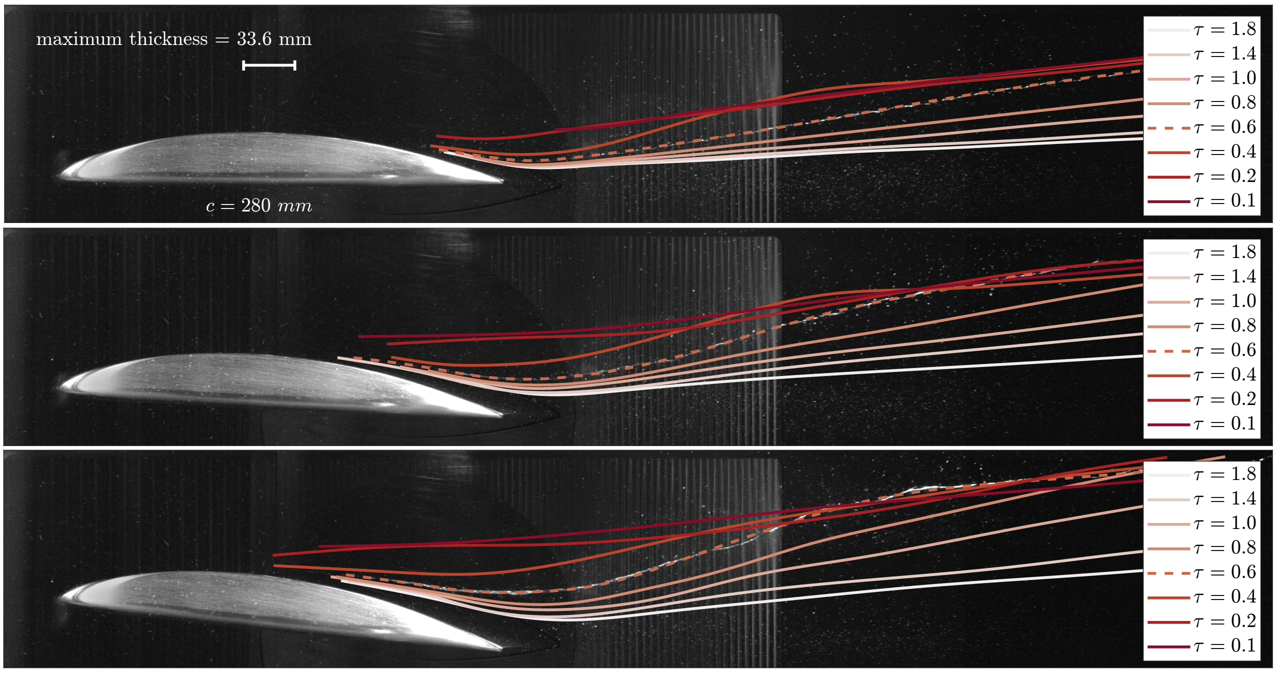


**Figure 3.** Trajectory of the leakage vortex for $\alpha = 0°$, $\alpha = 3°$, and $\alpha = 6°$ for varying $\tau$ with abundant cavitation nuclei for $\sigma = 6$.

expands downstream. If the local flow has been in a state of tension up to this point and two cavities meet, their union is followed by a momentary local cavity collapse. During these events a very loud acoustic impulse is emitted with pressure peaks reaching up to 2000 kPa. In contrast, in a flow with many weak freestream nuclei, tension within the flow does not develop. Instead of isolated/discrete events the flow is characterised by continual activation of nuclei close to the hydrofoil tip in the leakage vortex.

Starting from a large tip clearance, as $\tau$ is reduced the leakage vortex begins to deflect away from the trailing edge of the hydrofoil due to the presence of the wall and interactions with the wall boundary layer. The onset and development of this deflection with incidence is presented in figure 3. These trajectories were measured by examination of the high speed footage. For the seeded conditions at $\sigma = 6$ the maximum value of each pixel over successive frames was recorded until the trajectory of the vortex was apparent. In terms of the gap height, the $\delta_{99}$ boundary layer thickness corresponds to a ratio of $\tau = 0.57$. For $\tau$ near this value the the trajectory of the leakage vortex deviates strongly in the wake and changes quickly when below $\tau = 0.6$ to separate from the model closer to the tip.

To asses how the radiated acoustics in the filtered signal changes with tip clearance and cavitation number, the sound pressure level (SPL) for $\tau = \{0.1, 0.2, 0.4, 0.6, 0.8, 1.0, 1.4, 1.8\}$ are plotted in the top right quadrant for the three cavitation numbers featured in figure 4. For intermediate $\tau$ this results in extensive bubble excitation at high $\sigma$ and exacerbation of the strong acoustic collapse events described previously. When the gap is closed further, flow rate through the gap is reduced, as is the strength of the leakage vortex. This led to a peak in the SPL for the natural population that was observed to occur between $\tau \approx 0.5$–$1$. In the flow with abundant freestream nuclei this peak was only observed for high $\sigma$. At low $\tau$ and $\sigma$ in the abundant flow there remained regions of sufficient tension and unsteady flow that cavitation, and bubble fragmentation of the relatively weak nuclei that comprise the seeded population persisted.

During recording of the data the loud pressure spikes were very noticeable. To get a sense of the probability of these loud pressure peaks in the sparsely seeded flow, and the average pressure in the filtered signal, a histogram of instantaneous pressure values is plotted in the bottom right quadrant of figure 4. These data are plotted with two vertical axis scales. Plotted with a black line on a linear scale the average instantaneous pressure for each condition is apparent. In addition, by plotting these

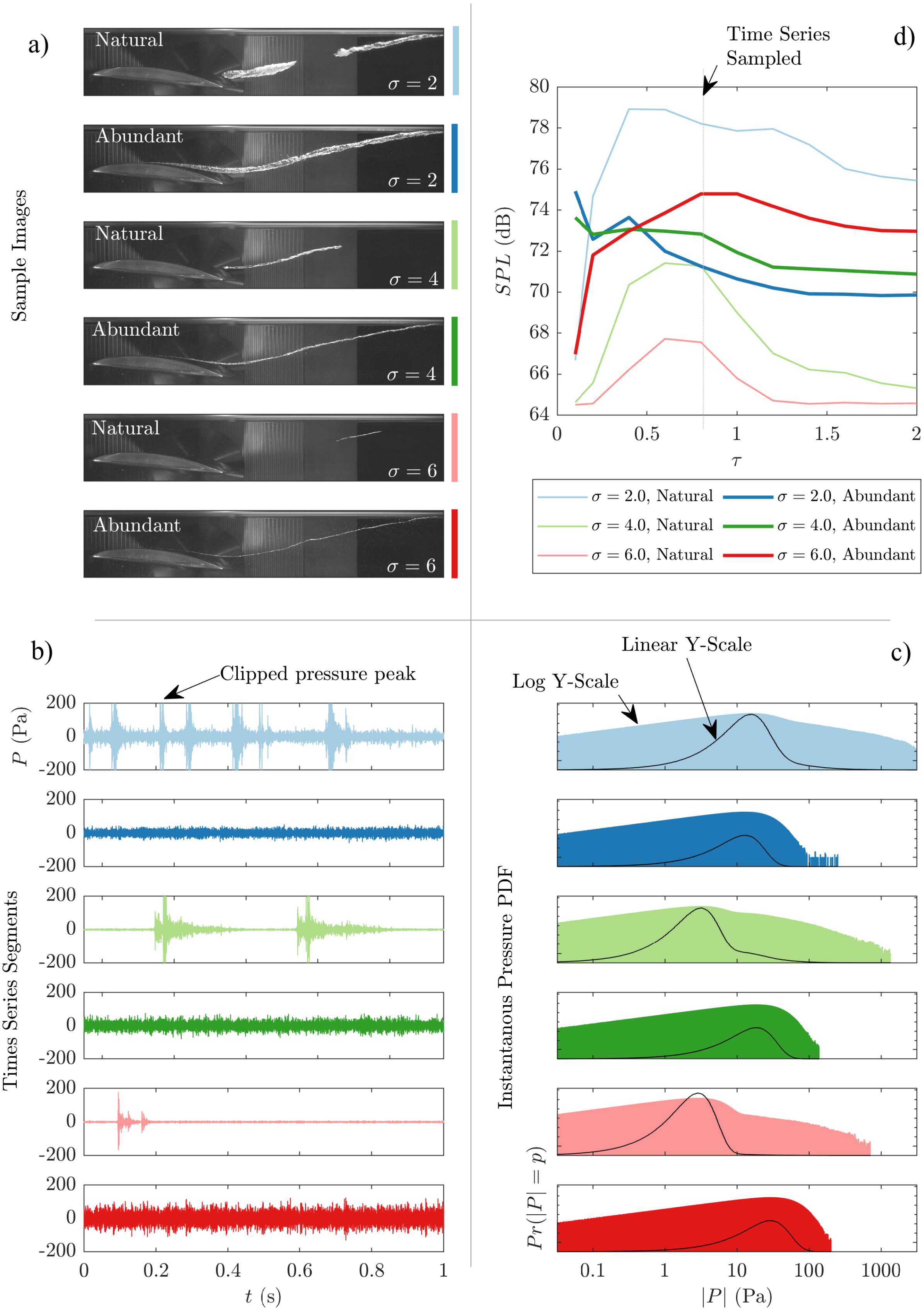


**Figure 4.** A comparison of cavitation topology and acoustic signature for $\sigma = 2,\ 4,\ 6\}$ and both the natural and abundant nuclei populations is presented. a) Sample images of the cavitation topology for each condition. b) Time series of acoustic pressure highpass filtered with a 1 kHz cutoff frequency. c) Probability density function for the instantaneous pressure in the highpass filtered acoustic data. The data are plotted on both a linear and logarithmic scale. d) The measured sound pressure level (SPL) of the acoustic data are plotted. Additionally, data for different tip height is now considered.

distributions with a logarithmic scale, rare but extremely loud events up to 100 times the average pressures are made visible. In the seeded flow, where there were plenty of nuclei to relieve tension, these peaks do not appear. With fewer activations the naturally populated flow was on average quieter, decreasing for higher cavitation numbers. In the abundantly seeded flow the instantaneous average pressure actually reduced with cavitation number for the $\alpha = 6^\circ$ case. As the tip leakage cavity diameter increased its surface exhibited fewer perturbations, and was concurrent with lower frequency and smaller amplitudes recorded in the acoustic data. It is important to keep these differences in mind when considering the sound pressure level measured in the flow. While on average the sound pressure level — an integrated measurement of the acoustic data — is higher for flow conditions with abundant nuclei, in a peak sense, even at the highest cavitation number ($\sigma = 6$) the instantaneous peaks in the sparse flow are louder than in the seeded flow at $\sigma = 2$. These differences highlight the importance of assessing the freestream nuclei content when designing and assessing tip leakage flow in pumps and ducted propulsors.

## 3 Conclusions

A comparison of cavitation topology and acoustic data for tip leakage flow with abundant and sparse poly-disperse nuclei populations has been presented. The acoustic characteristics change greatly with the freestream nuclei population. In the nuclei sparse flow significant tension can be sustained so that incipient and developed cavitation events alike produce loud spikes in acoustic pressure. In a abundantly nucleated flow these large instantaneous pressure are not observed due to the availability of nuclei to relieve tension in the flow, however the average sound pressure level is higher in the highly nucleated flow until cavitation within the flow is well developed. These features are modulated by the gap height and incidence of the hydrofoil. By comparing the trajectory of the nuclei and cavitation in the heavily seeded flow to the acoustic data, a peak in the radiated sound occurs at intermediate gap heights when the tip leakage vortex begins to interact with the wall boundary layer, deflecting the trajectory of the leakage vortex. Once flow through the gap reduces so too does the acoustic emissions in both nuclei populations tested near incipient conditions. The influence of nucleation was examined for the two extremes of nuclei populations in which turbo-machinery and ducted propulsors typically operate, and such an approach highlights the significant effects the nuclei population has on cavitation in the tip-leakage flows. Future efforts will concentrate on characterization of cavitation inception and dynamics across a range of intermediate poly-, and mono-disperse nuclei populations.

## Acknowledgements

This project was supported by the US Office of Naval Research and ONR Global through NICOP S&T Grant no. N62909-19-1-2062, and the 2019 U.S. Multidisciplinary University Research Initiative (MURI) and the Australian Defence Science and Technology Group (DSTG). The authors are grateful for the technical assistance provided by Mr. Steven Kent and Mr. Robert Wrigley when conducting these experiments.

## References

Barbaca, L., Russell, P.S., Pearce, B.W., Brandner, P.A., 2020. Characterization of microbubble generation in a confined turbulent jet. In *Proceedings of the 22nd Australasian Fluid Mechanics Conference*.

Brandner, P.A., Lecoffre, Y., Walker, G.J., 2006. Development of an australian national facility for cavitation research. In *In Sixth International Symposium on Cavitation - CAV 2006.*

Brandner, P.A., Lecoffre, Y., Walker, G.J., 2007. Design considerations in the development of a modern Cavitation Tunnel. In *Proceedings of the 16th Australasian Fluid Mechanics Conference, 16AFMC*. 630–637.

Chang, N.A., Choi, J., Yakushiji, R., Ceccio, S.L., 2012. Cavitation inception during the interaction of a pair of counter-rotating vortices. *Physics of Fluids*, **24**(1), 014107.

Chesnakas, C.J., Jessup, S.D., 2003. Tip-vortex induced cavitation on a ducted propulsor. In *Fluids Engineering Division Summer Meeting*. volume 36967, 257–267.

Doolan, C., Brandner, P., Butler, D., Pearce, B., Moreau, D., Brooks, L., 2013. Hydroacoustic characterization of the AMC cavitation tunnel. In *In Acoustic 2013, Victor Harbour, Australia*.

Dreyer, M., Decaix, J., Mönch-Alligné, C., Farhat, M., 2014. Mind the gap: a new insight into the tip leakage vortex using stereo-PIV. *Experiments in Fluids*, **55**(11), 1849.

Green, S.L., 1995. *Fluid Vortices*. Kluwer, Dodrecht, Netherlands.

Hsiao, C.T., Chahine, G.L., 2008. Numerical study of cavitation inception due to vortex/vortex interaction in a ducted propulsor. *Journal of Ship Research*, **52**(2), 114–123.

Khoo, M.T., Venning, J.A., Pearce, B.W., Takahashi, K., Mori, T., Brandner, P.A., 2020. Natural nuclei population dynamics in cavitation tunnels. *Experiments in Fluids*, **61**(2), 34. ISSN 1432-1114.

Laborde, R., Chantrel, P., Mory, M., 1997. Tip Clearance and Tip Vortex Cavitation in an Axial Flow Pump. *Journal of Fluids Engineering*, **119**(3), 680–685.

Oweis, G.F., Ceccio, S.L., 2005. Instantaneous and time-averaged flow fields of multiple vortices in the tip region of a ducted propulsor. *Experiments in Fluids*, **38**(5), 615–636.

Oweis, G.F., Fry, D., Chesnakas, C.J., Jessup, S.D., Ceccio, S.L., 2006a. Development of a tip-leakage flow-Part 2: Comparison between the ducted and un-ducted rotor. *Journal of fluids engineering*, **128**(4), 765–773.

Oweis, G.F., Fry, D., Chesnakas, C.J., Jessup, S.D., Ceccio, S.L., 2006b. Development of a Tip-Leakage Flow—Part 1: The Flow Over a Range of Reynolds Numbers. *Journal of Fluids Engineering*, **128**(4), 751–764.

Rains, D.R., 1954. *Tip clearance flows in axial compressors and pumps*. PhD Thesis.

Russell, P.S., Barbaca, L., A., V.J., Russell, E.S.C., Pearce, B.W., Brandner, P.A., 2020a. Cavitation in Tip-Leakage Flows. In *33rd Symposium on Naval Hydrodynamics*.

Russell, P.S., Barbaca, L., Venning, J.A., Pearce, B.W., Brandner, P.A., 2020b. Measurement of nuclei seeding in hydrodynamic test facilities. *Experiments in Fluids*, **61**(3), 79. ISSN 1432-1114.

Russell, P.S., Barbaca, L., Venning, J.A., Pearce, B.W., Brandner, P.A., 2020c. Nucleation effects on tip-gap cavitation. In *22nd Australasian Fluid Mechanics Conference (AFMC2020)*. 1–4.

Russell, P.S., Pearce, B.W., Brandner, P.A., 2022. A method for generating lifting surface profiles from simplified parametric equations. In *23rd Australasian Fluid Mechanics Conference - (23AFMC)*.

Temperley, H.N.V., Ll, G.C., 1946. The behaviour of water under hydrostatic tension: I. *Proceedings of the Physical Society*, **58**(4), 420.

Wu, H., Tan, D., Miorini, R.L., Katz, J., 2011. Three-dimensional flow structures and associated turbulence in the tip region of a waterjet pump rotor blade. *Experiments in Fluids*, **51**(6), 1721–1737.